Dokuz Eylül Üniversitesi Mühendislik Fakültesi Fen ve Mühendislik Dergisi
Dokuz Eylul University Faculty of Engineering Journal of Science and Engineering

Experimental investigations on the thermal performance of additively manufactured porous topologies

Eklemeli imal edilmiş gözenekli topolojilerin ısıl performansı üzerine deneysel incelemeler

Şahin Güngör [1*] 🆔

[1] Izmir Katip Celebi University Department of Mechanical Engineering, Izmir, TURKEY.
Sorumlu Yazar / Corresponding Author *: sahin.gungor@ikc.edu.tr

Abstract

Additive manufacturing enables researchers to form unique and unconventional topologies satisfying design compactness, improved efficiency, and lower cost. Design freedom introduced by the additive manufacturing reveals the idea of implementing the topology optimization approach into thermal systems. In this study, changes in thermal performance of three types of topologies: gyroid, hexagon (honeycomb), and rectilinear are experimentally investigated. In addition, porosity level of each topology is varied in between 25%, 50% and 75% to improve the impact of the study. The experimental results indicate that gyroid structures are thermally more efficient (up to 15.6%) than the remaining topologies. Furthermore, thermal diffusivities of the rectilinear and gyroid topologies with 25% porosity level are measured as the extremes, and it is detected that these structures propagate heat 1.1 times greater than the hexagon structure.

Keywords: Topology optimization, Porous media, Effective thermal conductivity, Thermal diffusivity.

Öz

Eklemeli üretim, araştırmacıların tasarım kompaktlığı, gelişmiş verimlilik ve düşük maliyeti sağlayan benzersiz ve sıra dışı topolojiler oluşturmasına imkân verir. Eklemeli üretimin getirdiği tasarım özgürlüğü, topoloji optimizasyon yaklaşımını ısıl sistemlere uygulama fikrini ortaya çıkarmaktadır. Bu çalışmada, üç farklı tip topoloji için ısıl performansındaki değişimi deneysel olarak araştırılmaktadır: gyroid, bal peteği ve doğrusal. Ek olarak, çalışmanın etkisini artırmak için her topolojinin gözeneklilik seviyesi %25, %50 ve %75 arasında değiştirilmektedir. Deneysel sonuçlar, jiroid yapıların diğer topolojilere kıyasla ısıl yönden daha verimli (%15.6'ya kadar)olduğunu göstermektedir. Ayrıca, %25 poroziteye sahip doğrusal ve jiroid topolojilerin termal yayınımları uç noktalar olarak ölçülmüştür ve bu yapıların altıgen yapıya göre 1.1 kat daha fazla ısı yaydığı tespit edilmiştir.

Anahtar Kelimeler: Topoloji optimizasyonu, Gözenekli yapı, Etkin ısıl iletkenlik, Isıl yayılım.

1. Introduction

Topology (shape) optimization contributes to design improved layouts under specific volume and boundary conditions [1, 2]. New softwares and tools propose diverse algorithms to generate topology optimization-based geometries or layouts [3-5], but manufacturing of these

structures is still a crucial problem. At this point, additive manufacturing technologies enable us to get high-quality products having unique or unconventional structures [6, 7]. As the product is created layer-by-layer, the final products need no more material removal process [8, 9]. This issue is the main superiority of the additive manufacturing technologies as it reduces the manufacturing cost by decreasing the total material consumption.

Mechanical performance of the 3D-printed topologies is studied in a comprehensive way in the stress distribution [10], specific stiffness [11], compression-bending [12] and fatigue [13] points of view. For instance, Ma et al. [14] investigated the impact of environmental conditions on the mechanical properties such as compressive and flexural strength. Likewise, Heever et al [15] considered the porosity effects on 3D-printed concrete domain. The findings indicated that the elasticity is dominated by porosity level. On the other hand, Rimasauskas et al. [16] parametrically studied the layer height and line width to observe the tensile properties. The results showed that mechanical performance of 3D printed composite structures can be improved by process parameters.

Although the literature contains many scientific papers related to the mechanical/material performance of the 3D printed topologies [17-21], main gap of the literature is the evaluation and experimental investigations of the thermal characteristics of additively manufactured structures. In the thermal engineering systems, the researchers mainly aim to enhance the conductance performance and thermal uniformity for conduction heat transfer applications having diverse topologies [22-25]. Furthermore, optimized heat transfer topologies have been rarely manufactured by the help of 3D printing technology [26-28]. In this study, the conduction heat transfer performance of the three different topologies: gyroid, hexagon (honeycomb), and rectilinear has been investigated. Thermal conductivity and thermal effusivity are determined as the output parameters of the experimental research. Porosity level is varied as 25%, 50% and 75% for the investigated topologies to observe the change in heat transfer performance. Furthermore, the thermal conductivity measurements of the 3D printed topologies are performed in x, y, z-directions to improve the impact of the study.

2. Material and Methods

In this study, gyroid, hexagon and rectilinear structures are experimentally examined in terms of thermal conductivity, effusivity and thermal diffusivity performance points of view. This section presents the manufacturing steps, boundary conditions, main assumptions, and experimental set-up configuration.

2.1. Additively Manufactured Topologies

Thermal conductivity and effusivity characteristics of additively manufactured gyroid, hexagon and rectilinear topologies are investigated at various porosity levels. The structures are manufactured in the volume of 30-mm cube via a professional 3D printer. Figure 1 presents cross-sections of the investigated topologies. The presented topologies are three-dimensional, and the figures are captured from the front view. The void volume of the hexagon structure (Fig. 2b) appears to be less; however, this is due to an optical delusion.
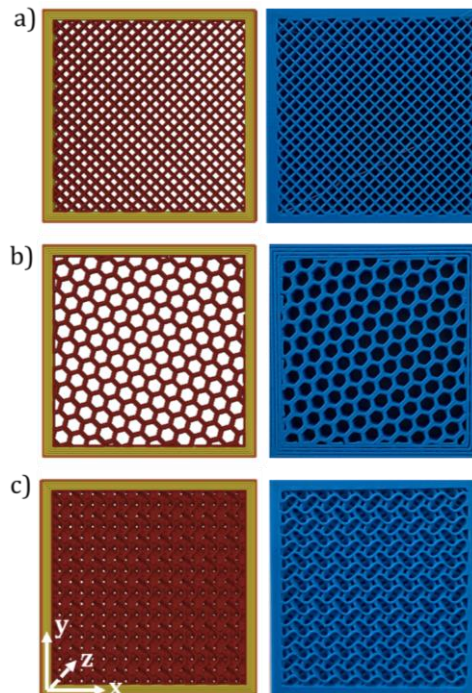
Figure 1. Investigated and manufactured topologies, a) rectilinear, b) hexagon (honeycomb), and c) gyroid.

The manufacturing tolerance and layer thickness of the 3D printer is ±0.1 mm and 0.4 mm, respectively. The structures with 25%, 50% and

75% porosity levels are manufactured in one printing step to avoid from the environmental irreversibilities. Note that the ambient temperature during the manufacturing processes is maintained at about 20 ºC.

Figure 2 shows the 3D printer and manufactured structures based on the polylactic acid (PLA) material. Once high-quality structures at different porosity values have been manufactured, thermal performance of these topologies is investigated in the thermal conductivity, effusivity and diffusivity points of view.

Figure 2. 3D printer and a view from the manufactured topologies.

2.2. Conductivity and Effusivity Experiments

In the experimental investigations, C-Therm TCI analyzer is utilized for precisely measuring the thermal conductivity, effusivity and thermal diffusivity. The operating temperature range of the device varies between -50ºC and 200ºC. Note that all the experimental investigations comply with the ASTM D7984 transient plane source standards with a measurement tolerance of less than ±1 %. The device has one-sided heat reflectance sensor with a heating domain.

The heating element is supported by an insulated backing. Applied current causes simultaneous heat generation within the heating element (coil). As the backside of the heating element is insulated, generated heat is only transferred in the reverse direction, and this operation creates temperature increase.
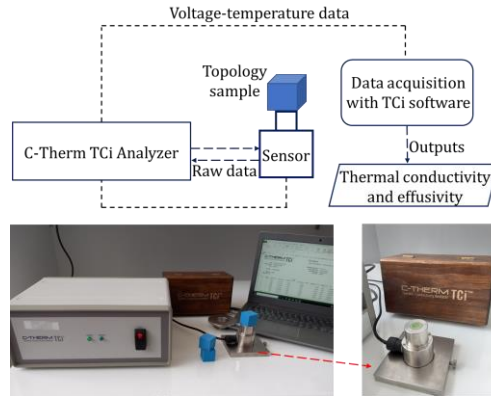
Figure 3. The experimental setup configuration.

Figure 3 presents the experimental setup used for measuring the thermal conductivity and thermal effusivity. Temperature variation is basically monitored by the voltage change of the calibrated main sensor. The thermal conductivity measurements in the experimental setup is based on the Fourier's Law [29, 30]:

$$Q = kA_s \frac{dT}{dn} \quad , in\ the\ unit\ of\ [W] \qquad (1)$$

where, Q is the conduction heat transfer rate, k denotes the thermal conductivity of the investigated materials, A_s is the heat transfer surface area, T is the abbreviation of temperature, and n is the length in the investigated axis. On the other hand, thermal effusivity (responsivity) corresponds the thermal energy exchange capability of the structure with its ambient [31, 32]. Thermal effusivity of an investigated topology can be calculated as:

$$e = \left(k\rho C_p\right)^{0.5}, in\ the\ unit\ of\ \left[\frac{Ws^{0.5}}{m^2 K}\right] \qquad (2)$$

Here, e is the thermal effusivity, ρ and C_p are the material density and the specific heat capacity, respectively. Likewise, the thermal diffusivity was measured to report the rate of heat propagation driven by the conduction heat transfer. The thermal diffusivity of the system is as follows:

$$\alpha = {k}/{\rho C_p} \quad , in\ the\ unit\ of\ \left[\frac{m^2}{s}\right] \qquad (3)$$

In the experimental setup, temperature increase in the system is inversely proportional with the thermal conductivity of the material. The physical reason behind this issue is the constant

heat flux applied by the heating element. Note that the experimental setup allows us to repeat the experiments for preventing the ambiguity or uncertainty problems. Therefore, same experiments were conducted at least for ten iterations to obtain more accurate results.

3. Experimental Results

In this paper, thermal performance of additively manufactured structures at various porosity levels are experimentally investigated. Table 1 presents the thermal conductivity and effusivity results of the gyroid topology when the structure porosity is 25%, 50%, and 75%. Gyroid is a triply periodic minimal surface (TPMS) having high heat transfer surface area compared to the total volume.

Table 1. Three dimensional thermal characteristics for the gyroid structure.

Gyroid 25% porosity	Thermal conductivity [W/mK]	Thermal effusivity [W$s^{0.5}/m^2K$]
x-direction	0.380	784
y-direction	0.374	753
z-direction	0.292	496
50% porosity	Thermal conductivity [W/mK]	Thermal effusivity [W$s^{0.5}/m^2K$]
x-direction	0.367	728
y-direction	0.369	733
z-direction	0.273	431
75% porosity	Thermal conductivity [W/mK]	Thermal effusivity [W$s^{0.5}/m^2K$]
x-direction	0.365	727
y-direction	0.342	679
z-direction	0.261	395

As the porosity corresponds to void volume within a structure, greater porosity causes more air gaps and lower thermal conductivity, as expected. Table 1 shows the variation of thermal conductivity and effusivity for each direction given in Fig. 2. Lower conductivity was observed from the front surface of the gyroid structures (z-direction) in every porosity levels. Furthermore,

both the thermal effusivity and thermal conductivity decreases in more porous structures. Likewise, Table 2 presents the same thermal parameters for the hexagon topologies at various porosity levels. The trend of change is similar to the gyroid structure, yet the thermal conductivity values are less than the level of the gyroid topology.

Table 2. Thermal conductivity and effusivity of the hexagon structure.

Hexagon 25% porosity	Thermal conductivity [W/mK]	Thermal effusivity [W$s^{0.5}/m^2K$]
x-direction	0.361	723
y-direction	0.319	635
z-direction	0.257	418
50% porosity	Thermal conductivity [W/mK]	Thermal effusivity [W$s^{0.5}/m^2K$]
x-direction	0.346	699
y-direction	0.311	612
z-direction	0.239	388
75% porosity	Thermal conductivity [W/mK]	Thermal effusivity [W$s^{0.5}/m^2K$]
x-direction	0.313	632
y-direction	0.298	547
z-direction	0.226	365

Main reason behind the lower thermal parameters of the hexagon structures is the longer vertical and horizontal spacings behaving as an insulation. The next investigated topology is the rectilinear path having more homogenous distribution within the structures. Table 3 shows the thermal conductivity and effusivity results in each direction of the rectilinear topologies. The experimental findings indicate that rectilinear structures are thermally more conductive than hexagon topologies. Furthermore, thermal conductivity results of the rectilinear topologies in x and y-directions are very close to each other at each porosity level. This causes due to the almost symmetric paths in x and y directions (see Fig. 2a). The z-direction (front view) has more impact on both thermal conductivity and

effusivity measurements for 25%, 50%, and 75% porous rectilinear structures.

Table 3. Thermal characteristics for the rectilinear structure.

Rectilinear *25% porosity*	Thermal conductivity [*W/mK*]	Thermal effusivity [Ws$^{0.5}$/m^2K]
x-direction	0.377	766
y-direction	0.375	758
z-direction	0.282	469
50% porosity	Thermal conductivity [W/mK]	Thermal effusivity [Ws$^{0.5}$/m^2K]
x-direction	0.339	677
y-direction	0.341	670
z-direction	0.240	419
75% porosity	Thermal conductivity [W/mK]	Thermal effusivity [Ws$^{0.5}$/m^2K]
x-direction	0.327	604
y-direction	0.330	615
z-direction	0.214	396

On the other hand, thermal diffusivity is another critical parameter presenting the conduction based thermal propagation performance of a topology. Variations in the thermal diffusivity are also reported for all the investigated topologies and porosity levels. In Figure 4, average thermal conductivity and thermal diffusivity results are documented for the gyroid, hexagon and rectilinear topologies, respectively. Here the parameter of density by specific heat capacity is taken from the experimental measurements. As thermal diffusivity directly depends on the thermal conductivity, the thermal diffusivity increases with decrement in the porosity level. The experimental results indicate that gyroid structure with 25% porosity level propagates heat in a more efficient way by the contribution of conductive heat transfer. Furthermore, the thermal diffusivity level of the rectilinear structure at the same porosity level detected as very close to the maximum measured thermal diffusivity value. On the other hand, minimum thermal diffusivity is measured at hexagon structure with 75% porosity level.
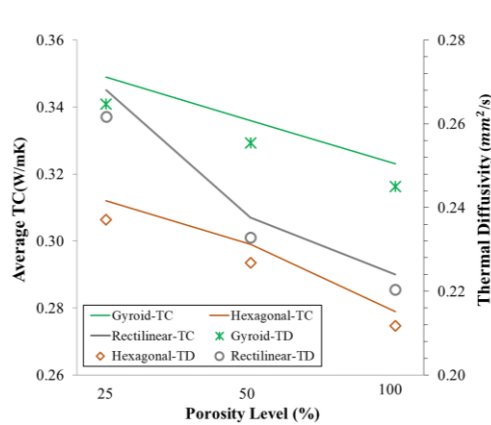
Figure 4. Variation of the average thermal conductivity (TC) and thermal diffusivity (TC) levels with respect to porosity level of each investigated topology.

An additional analysis is performed to check the uncertainty level of the experimental measurements to determine the robustness and accuracy of the system. Monte Carlo method is utilized for the calculation of measurement errors [33, 34]. The gyroid structure at 25% porosity level is selected as sample, and ten measurements in y-direction have been conducted at identical boundary and initial conditions. Maximum, mean, and minimum measurement values are documented for both thermal conductivity and thermal effusivity parameters.

Table 4. Uncertainty analysis results.

Gyroid *25% porosity*	Thermal conductivity [*W/mK*]	Thermal effusivity [Ws$^{0.5}$/m^2K]
Max. value	0.3792	756.8
Mean value	0.3741	753.3
Min. value	0.3721	750.9

Table 4 shows the uncertainty analysis results after ten identical experiments. The findings indicate that although the thermal conductivity device manufacture claims the measurements are in a range of ± 1% tolerance, the uncertainty level may reach up to ± 1.9%.

4. Discussion and Conclusion

In this paper, thermal performance and characteristics of additively manufactured structures at various porosity levels have been

experimentally investigated. Three different topologies of rectilinear, hexagon (honeycomb) and gyroid are determined as the main paths within the structures. High-quality 3D printer technology is utilized to manufacture the investigated topologies at 25%, 50%, and 75% porosity levels. The topologies are experimentally examined via a professional device to measure the thermal conductivity and thermal effusivity values. The experiments are repeated at least ten times for preventing the ambiguity or uncertainty problems. The ambient temperature and environmental conditions are kept the same both in the manufacturing steps and during the experiments. Main findings are given as follows:

- The gyroid structures at all porosity levels are thermally more conductive than the rectilinear and hexagonal topologies.

- Enhancement in the thermal conductivity reaches up to 21.9% among the 75% porous gyroid and rectilinear structures (z-direction).

- Investigated rectilinear and gyroid topologies at 25% porosity level provide maximum thermal diffusivities ($\simeq 0.26$ mm^2/s) in the experiments.

- Thermal propagation performance of the gyroid structure is up to 15.6% higher than the hexagonal topology.

In the near future, these topologies are expected to be modelled numerically to apply into thermal-fluid engineering problems under various boundary-initial conditions.

5. Ethics committee approval and conflict of interest statement

"Ethics committee approval is not required for the prepared article"

"There is no conflict of interest with any person/institution in the prepared article"

Acknowledgment

References

[1] Rong, Y., Zhao, Z.L., Feng, X.Q., Xie Y.M. 2022. Structural topology optimization with an adaptive design domain. Computer Methods in Applied Mechanics and Engineering. Volume 389, 114382. https://doi.org/10.1016/j.cma.2021.114382

[2] Prathyusha, A.L.R., Babu, G.R. 2022. A review on additive manufacturing and topology optimization process for weight reduction studies in various industrial applications. Materials Today Proceedings. Volume 62, pp. 109-117. https://doi.org/10.1016/j.matpr.2022.02.604

[3] Fawaz, A., Hua, Y., Le Corre, S., Fan, Y., Luo, L. 2022. Topology optimization of heat exchangers: A review. Energy, Volume 252, 124053. https://doi.org/10.1016/j.energy.2022.124053

[4] Lopes, H.N., Cunha, D.C., Pavanello, R., Mahfoud, J. 2022. Numerical and experimental investigation on topology optimization of an elongated dynamic system. Mechanical Systems and Signal Processing. Volume 165, 108356. https://doi.org/10.1016/j.ymssp.2021.108356

[5] Sun, Z., Wang, Y., Liu, P., Luo, Y. 2022. Topological dimensionality reduction-based machine learning for efficient gradient-free 3D topology optimization. Materials & Design. Volume 220, 110885. https://doi.org/10.1016/j.matdes.2022.110885

[6] Bujny, M., Olhofer, M., Aulig, N., Duddeck, F. 2021. Topology Optimization of 3D-printed joints under crash loads using Evolutionary Algorithms. Structural and Multidisciplinary Optimization. Volume 64, pp. 4181–4206. https://doi.org/10.1007/s00158-021-03053-4

[7] Siegkas, P. 2022. Generating 3D porous structures using machine learning and additive manufacturing. Materials & Design. Volume 220, 110858. https://doi.org/10.1016/j.matdes.2022.110858

[8] Shuaib, M., Haleem, A., Kumar, S., Javaid, M. 2021. Impact of 3D Printing on the environment: A literature-based study. Sustainable Operations and Computers. Volume 2, pp. 57-63. https://doi.org/10.1016/j.susoc.2021.04.001

[9] Maleki, E., Bagherifard, S., Bandini, M., Guagliano, M. 2021. Surface post-treatments for metal additive manufacturing: Progress, challenges, and opportunities. Additive Manufacturing. Volume 37, 101619. https://doi.org/10.1016/j.addma.2020.101619

[10] Lu, J., Dong, P., Zhao, Y., Zhao, Y., Zeng, Y., 2021. 3D printing of TPMS structural ZnO ceramics with good mechanical properties. Ceramics International. Volume 47, 12897-12905. https://doi.org/10.1016/j.ceramint.2021.01.152

[11] Kushwaha, B., Dwivedi, K., Ambekar, R.S., Pal, V., Jena, D.P., Mahapatra, D.R., Tiwary, C.S. 2020. Mechanical and acoustic behavior of 3D-printed hierarchical mathematical fractal menger sponge. Advance Engineering Materials. Volume 23, 2001471. https://doi.org/10.1002/adem.202001471

[12] Rouf, S., Rina, A., Haq, M.I.U., Naveed, N., Jeganmohan, S., Kichloo, A.F. 2022. 3D printed parts and mechanical properties: Influencing parameters, sustainability aspects, global market scenario, challenges, and applications. Advanced Industrial and Engineering Polymer Research. Volume 5, 143-158. https://doi.org/10.1016/j.aiepr.2022.02.001

[13] Afrose, M.F., Masood, S.H., Iovenitti, P., Nikzad, M., Sbarski, I. 2016. Effects of part build orientations on fatigue behaviour of FDM-processed PLA material.

Progress in Additive Manufacturing. Volume 1, 21–28. https://doi.org/10.1007/s40964-015-0002-3.

[14] Ma, L., Zhang, Q., Jia, Z., Liu, C., Deng, Z., Zhang, Y. 2022. Effect of drying environment on mechanical properties, internal RH and pore structure of 3D printed concrete. Construction and Building Materials. Volume 315, 125731. https://doi.org/10.1016/j.conbuildmat.2021.125731

[15] Heever, M., Plessis, A., Kruger, J., Zijl, G. 2022. Evaluation the effects of porosity on mechanical properties of extrusion-based 3D printed concrete. Cement and Concrete Research. Volume 153, 106695.
https://doi.org/10.1016/j.cemconres.2021.106695

[16] Rimasauskas, M., Jasiuniene, E., Kuncius, T., Rimasauskiene, R., Cicenas, V. 2022. Investigation of influence of printing parameters on the quality of 3D printed composite structures. Composite Structures. Volume 281, 115061. https://doi.org/10.1016/j.compstruct.2021.115061

[17] Zhang, Y., Hsieh, M.T., Valdevit, L. 2021. Mechanical performance of 3D printed interpenetrating phase composites with spinodal topologies. Composite Structures. Volume 263, 113693. https://doi.org/10.1016/j.compstruct.2021.113693

[18] Indres, A.I., Constantinescu, D.M., Mocian, O.A. 2021. Bending behavior of 3D printed sandwich beams with different core topologies. Wiley Material Design & Processing Communications. Volume 3, e252. https://doi.org/10.1002/mdp2.252

[19] Jeong, D.G., Seo, H.S. 2021. Study on mechanical performance of 3D printed composite material with topology shape using finite element method. Functional Composites and Structures. Volume 3, 035003.
https://doi.org/10.1088/2631-6331/ac1914

[20] Hmeidat, N.S., Brown, B., Jia, X., Vermaak, N., Compton, B. 2021. Effects of infill patterns on the strength and stiffness of 3D printed topologically optimized geometries. Rapid Prototyping Journal, Volume 27, pp. 1467-1479. https://doi.org/10.1108/RPJ-11-2019-0290

[21] Zhang, J., Yanagimoto, J. 2021. Density-based topology optimization integrated with genetic algorithm for optimizing formability and bending stiffness of 3D printed CFRP core sandwich sheets. Composites Part B: Engineering. Volume 225, 109248.
https://doi.org/10.1016/j.compositesb.2021.109248

[22] Ozguc, S., Pan, L., Weibel, J.A. 2021. Topology optimization of microchannel heat sinks using a homogenization approach. International Journal of Heat and Mass Transfer, Volume 169,120896. https://doi.org/10.1016/j.ijheatmasstransfer.2020.120896.

[23] Dirker, J., Meyer, J.P. 2013. Topology Optimization for an Internal Heat-Conduction Cooling Scheme in a Square Domain for High Heat Flux Applications. Journal of Heat Transfer, ASME. Volume 135, 111010. https://doi.org/10.1115/1.4024615

[24] Donoso, A. 2006. Numerical Simulations in 3D Heat Conduction: Minimizing the Quadratic Mean Temperature Gradient by an Optimality Criteria Method. SIAM Journal on Scientific Computing, Volume 28, pp. 929-941. https://doi.org/10.1137/060650453

[25] Dbouk, T. 2017. A review about the engineering design of optimal heat transfer systems using topology optimization. Applied Thermal Engineering. Volume 112, 841-854. https://doi.org/10.1016/j.applthermaleng.2016.10.134.

[26] Li, H., Ding, H., Meng, F., Jing, D., Xiong, M. 2019. Optimal design and thermal modelling for liquid-cooled heat sink based on multi-objective topology optimization: An experimental and numerical study. International Journal of Heat and Mass Transfer. Volume 144, 118638. https://doi.org/10.1016/j.ijheatmasstransfer.2019.118638

[27] Taha, B., Patil, S., Dennis, B.H. 2021. Design and Manufacturing of Topology Optimized Heat Sinks Made of Copper Using 3D Printing. ASME Proceedings of the 16th International Manufacturing Science and Engineering Conference. Volume 1: Additive Manufacturing. June 21–25. https://doi.org/10.1115/MSEC2021-63877

[28] Tseng, P.H., Tsai, K.T., Chen, A.L., Wang, C.C. 2019. Performance of novel liquid-cooled porous heat sink via 3D laser additive manufacturing. International Journal of Heat and Mass Transfer. Volume 137, 558-564.https://doi.org/10.1016/j.ijheatmasstransfer.2019.03.116

[29] Bejan, A. 2013. Convection Heat Transfer. 4th Edition. WILEY, Hoboken, New Jersey.

[30] Cengel, Y.A. 2002. Heat Transfer: A Practical Approach. 2nd Edition. McGraw-Hill, New York.

[31] Incropera, F.P., Dewitt, D.P., Bergman, T.L., Lavine, A.S. 2020. Principles of Heat and Mass Transfer. Global Edition. WILEY, Hoboken, New Jersey.

[32] Oss. S. 2022. A simple model of thermal conduction in human skin: temperature perception and thermal effusivity. European Journal of Physics, Volume 43, 035101.
https://doi.org/10.1088/1361-6404/ac4c8a

[33] Turhan, C., Ceter, A.E. 2021. A novel occupant detection-based ventilation control strategy for smart building applications. Mugla Journal of Science and Technology. Volume 7, pp. 24-35. https://doi.org/10.22531/muglajsci.928315

[34] Turhan, C. 2020. Comparison of indoor air temperature and operative temperature driven HVAC systems by means of thermal comfort and energy consumption. Mugla Journal of Science and Technology. Volume 6, pp. 156-163. https://doi.org/10.22531/muglajsci.679256